



# A colorimetric sensing platform with smartphone for organophosphorus pesticides detection based on PANI-MnO<sub>2</sub> nanozyme

Cheng-Lin Yang<sup>a</sup>, Li-Hong Yu<sup>a</sup>, Yue-Hong Pang<sup>a,b</sup>, Xiao-Fang Shen<sup>a,b,\*</sup>

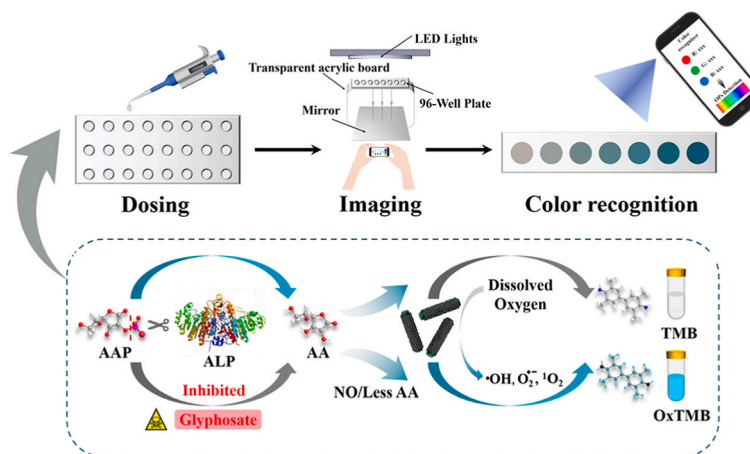
<sup>a</sup> State Key Laboratory of Food Science and Resources, School of Food Science and Technology, Collaborative Innovation Center of Food Safety and Quality Control in Jiangsu Province, Jiangnan University, Wuxi 214122, China

<sup>b</sup> International Joint Laboratory on Food Safety, Jiangnan University, Wuxi 214122, China

## HIGHLIGHTS

- PANI-MnO<sub>2</sub> with mild preparation conditions exhibits excellent oxidase-like activity.
- PANI-MnO<sub>2</sub>-based colorimetry was established for organophosphorus pesticide detection.
- A colorimetric platform was fabricated for instrument-free detection.
- This proposed method can be applied in environment and food samples.

## GRAPHICAL ABSTRACT



## ARTICLE INFO

Handling Editor: Dr. J.P. Landers

**Keywords:**  
 PANI-MnO<sub>2</sub> nanocomposites  
 Nanozyme  
 Organophosphorus pesticides  
 Colorimetric detection  
 Smartphone

## ABSTRACT

Organophosphorus pesticides (OPs) are of great concern due to its potential harms on human health and the environment. Herein, a budget-friendly, rapid and convenient colorimetric sensing platform is developed for detection of OPs in the environmental and food samples. The sensing element, PANI-MnO<sub>2</sub> nanozyme with excellent oxidase mimetic activity is synthesized at room temperature, which is able to directly oxidize 3,3',5,5'-tetramethylbenzidine (TMB) to generate blue colored oxidized TMB (OxTMB) within 2 min. Ascorbic acid (AA) can inhibit the oxidization reaction of TMB, consequently causing the blue color fading. Ascorbic acid 2-phosphate (AAP) could be hydrolyzed to produce AA by alkaline phosphatase (ALP). In the presence of OPs can effectively decrease ALP activity, resulting in the recovery of catalytic activity of PANI-MnO<sub>2</sub>. Therefore, sensitive and selective OPs detection is achieved. Under the optimal conditions, excellent detection performance in term of glyphosate as a model is achieved with a linear range from 0.50 to 50 μM, the detection limit is 0.39 μM (S/N = 3). The utility of method is further improved by combining a portable smartphone platform with a color

\* Corresponding author State Key Laboratory of Food Science and Resources, School of Food Science and Technology, Collaborative Innovation Center of Food Safety and Quality Control in Jiangsu Province, Jiangnan University, Wuxi 214122, China

E-mail address: [xfshen@jiangnan.edu.cn](mailto:xfshen@jiangnan.edu.cn) (X.-F. Shen).

<https://doi.org/10.1016/j.aca.2023.342045>

Received 9 October 2023; Received in revised form 15 November 2023; Accepted 17 November 2023

Available online 20 November 2023

0003-2670/© 2023 Elsevier B.V. All rights reserved.

picking application. The colorimetric platform achieves instrument-free detection of OPs and overcomes the uneven color distribution of traditional paper-based chip, providing an alternative strategy for the qualitative discernment and semi-quantitative analysis of OPs on-site.

## 1. Introduction

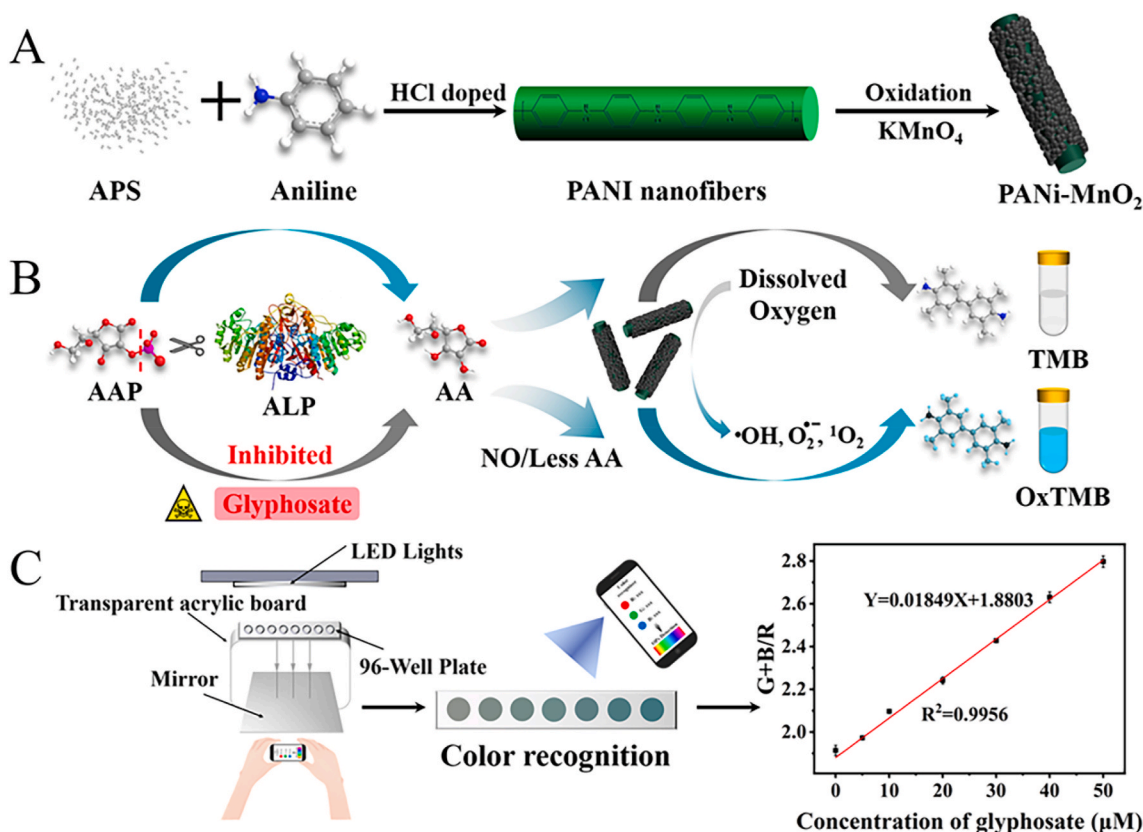
Organophosphorus pesticides (OPs) are widely used for pest control in the agriculture industry around the world due to their broad-spectrum insecticide activity and effectiveness [1]. However, due to OPs are not susceptible to degradation and inappropriate use, pesticide residues are an increasing threat to ecological environment and food safety [2,3]. Therefore, the monitoring of OPs in environmental and food samples is extremely significant. Until now, enzyme-linked immunosorbent assay (ELISA) [4], capillary electrophoresis (CE) [5], gas chromatography (GC) and high performance liquid chromatography (HPLC) or chromatography separation coupled with mass spectrometry (MS) detection, have been popularly used to detect OPs, these methods are generally able to distinguish various pesticides with high sensitivity and specificity [6–8]. Nevertheless, they are expensive, cumbersome, time-consuming and rely on complicated instrumentation and highly trained manpower, which limit their application for detection of OPs in on-site resource-limited situations [9].

Recently, the colorimetric strategy has been considered a promising method for the detection of OPs because of its fast response, direct observation with the naked eye and easy-operation [10]. Advanced functional nanomaterials with high specificity or catalytic properties are critical in the development of colorimetric sensor. To date, lots of functional nanomaterials such as Fe–N/C SAzymes [9], Mn–ZnS QD-MIP [10], Fe–Co MNPs/Fe–N–C [11], have been established for the detection of OPs. However, many nanomaterials are subjected to high temperature synthesis and complex multistep steps. Therefore, the synthesis of

functional nanomaterials using simple and convenient methods under milder conditions for detection of OPs is still highly desirable, particularly from simple and readily available starting materials.

Nanozymes with intrinsic enzyme-mimetic properties have attracted significant attention in analytical chemistry, because they can easily overcome some of the main disadvantages of natural enzymes such as instability, high cost and poor reproductivity [12,13]. In recent years, concerns related to oxidase-like nanozymes have been increased in the catalysis related fields due to no need of  $\text{H}_2\text{O}_2$  in the oxidase mimic-catalyzed reaction systems [14]. Materials containing noble metals are commonly used as oxidase-like nanozymes for catalyzed reactions, but the limited scarce reserves and high cost cannot support their practical applications [15]. Therefore, it is crucial to exploit non-noble metal-based nanozymes as alternatives. The catalytic property of manganese oxides in oxidase-like nanozymes catalyzed reactions was excellent due to their unique redox features, various structures and ease of synthesis [16,17]. Zhang et al. [15] reported oxidase mimetics (the wire-like  $\text{MnO}_2$ , rod-like  $\text{MnOOH}$  and octahedral-like  $\text{Mn}_3\text{O}_4$ ) could be controllably synthesized. Wan et al. [16] compared the  $\text{MnO}_2$  oxidase-like catalytic activity of five different morphologies (nanosphere, nanosheet, nanowire, nanostick and nanocomplex). Nevertheless, there is still limited research on approaches to synthesis of manganese oxides nanozymes with composite structure. Thus, it is highly desired to control synthesis of manganese oxides nanomaterials with various composites and structures and further understanding of their potential applications for biocatalysts and biosensing.

Polyaniline (PANI) is an organic material with extended conjugated  $\pi$



**Scheme 1.** Principle of colorimetric sensing for glyphosate detection based on the oxidase mimicking property of PANI-MnO<sub>2</sub>.

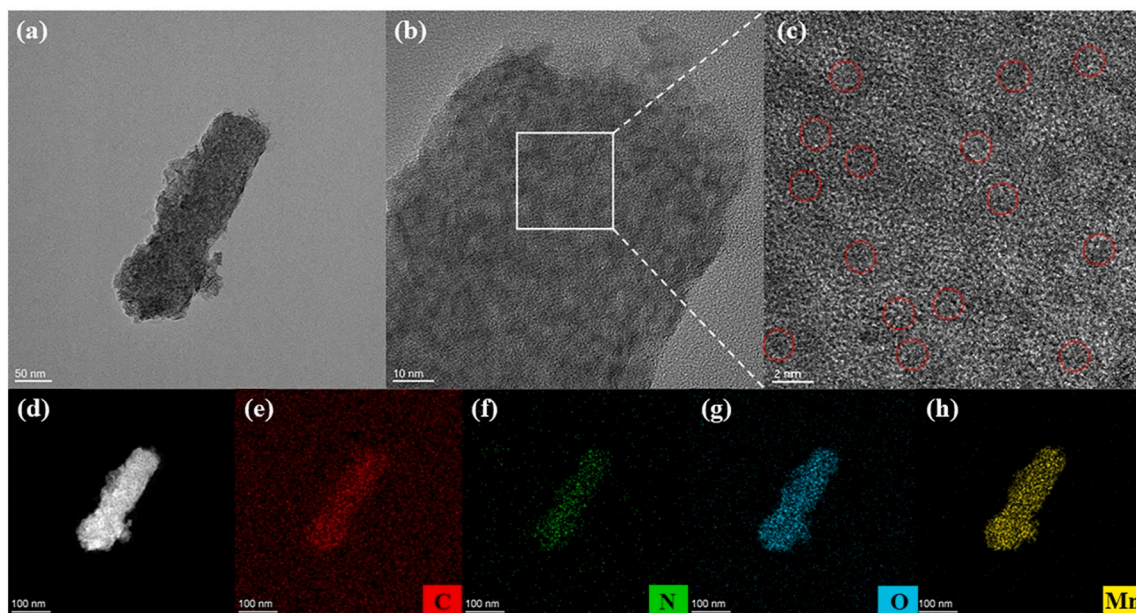


**Fig. 1.** (a) TEM micrograph of the PANI-MnO<sub>2</sub>; (b) HR-TEM micrograph of the PANI-MnO<sub>2</sub>; The lattice fringes of MnO<sub>2</sub> nanoparticles in (c) are highlighted by red circles.; (d) HAADF-STEM micrograph of the PANI-MnO<sub>2</sub>; (e–h) The elemental mapping of C, N, O and Mn of the PANI-MnO<sub>2</sub>. (For interpretation of the references to color in this figure legend, the reader is referred to the Web version of this article.)

bonds [18]. Due to their ease of synthesis, high electrical conductivity, good chemical stability and easy functionalization, they can be widely used in various fields including chemical sensors, batteries, supercapacitors, catalysis, and so on [19–21]. In particular, when PANI interacts with inorganic materials, the synergistic effect between composite materials can improve their electrical, optical, and catalytic properties [22]. In the past dozen years, a series of PANI composites (such as PANI/Cu<sub>9</sub>S<sub>5</sub> composite nanowires, PANI/Au hybrids, composite NiFe<sub>2</sub>O<sub>4</sub>-PANI) have been prepared and used as efficient peroxidase mimics [23–25]. However, research on conductive polymer nanocomposites mainly focused on preparation of peroxidase mimics. Therefore, it is of value to explore the formation, catalytic mechanism, and potential analytical applications of oxidase mimetics, which are made of manganese oxides and conductive polymer.

Herein, the PANI-MnO<sub>2</sub> is synthesized by a facile one-step self-assembly redox polymerization method, the formation and catalytic mechanism of the PANI-MnO<sub>2</sub> are systematically discussed. A simple, rapid and low-cost colorimetric method has been developed for OPs detection based on PANI-MnO<sub>2</sub>. By portable colorimetric platform, the results of uniform color distribution can be directly observed by smartphone applications. Our developed method contains sensitive response and portable device, thus offering a novel strategy for the on-site detection of OPs in the real samples.

## 2. Experiment

### 2.1. Design of the smartphone-based colorimetric platform for detection of glyphosate

As illustrated in Scheme 1A, PANI were prepared by rapid mixing reaction. Then, PANI were used as carriers and reducing agents, attachment of the MnO<sub>2</sub> nanoparticles to the its surface via oxidation reaction with the KMnO<sub>4</sub>, obtaining PANI-MnO<sub>2</sub>, all synthetic steps were conducted at room temperature. The prepared PANI-MnO<sub>2</sub> exhibited excellent oxidase-like activity and can oxidize colorless 3,3',5,5'-tetramethylbenzidine (TMB) to produce blue products (OxTMB). After adding ascorbic acid 2-phosphate (AAP) and alkaline phosphatase (ALP), AAP can be hydrolyzed by ALP to produce ascorbic acid (AA). The

generated AA can reduce the generation of oxidized TMB, causing significant blue fading. The addition of glyphosate irreversibly inhibited the activity of ALP, leading to the recovery of TMB color reaction (Scheme 1B). In order to realize the portable detection of glyphosate, a colorimetric sensing platform based on PANI-MnO<sub>2</sub> was prepared. After addition of glyphosate, TMB chromogenic reaction occurred in 96-well plate, the color can be recognized by a smartphone colorimetric platform, on-site detection of glyphosate can be made by comparing the RGB difference values (Scheme 1C).

### 2.2. Synthesis of PANI-MnO<sub>2</sub>

PANI was synthesized according to previous reports, with slight modifications [26]. Briefly, aniline (6.4 mmol) was dissolved in HCl solution (1 M, 20 mL), and then ammonium peroxydisulfate (1.6 mmol) was dispersed in the same HCl solution. Both solutions were rapidly mixed and incubated for 90 min at 25 °C. The blackish green product was centrifuged at 10000 rpm for 10 min to separate the precipitate of PANI. This precipitate was subsequently washed with ultrapure water and anhydrous ethanol, and then dried at 60 °C for 12 h.

PANI-MnO<sub>2</sub> was synthesized based on the reduction method with slight modifications [27]. 40 mg PANI was dispersed in 30 mL ultrapure water and sonicated for 30 min, and then this solution was added with 10 mL 2-morpholinoethanesulfonic acid (10 mM, pH 6.0) and 10 mL KMnO<sub>4</sub> (25 mM), and the mixture was stirred for 1 h at room temperature. The black product was centrifuged at 10000 rpm for 10 min to separate the precipitate of PANI-MnO<sub>2</sub>. This precipitate was subsequently washed with ultrapure water and anhydrous ethanol, and then dried at 60 °C for 12 h.

For comparison, MnO<sub>2</sub> and MnO<sub>2</sub> nanosheets were synthesized according to previous reports [28,33].

### 2.3. Investigation of oxidase-like mimetic activity

The oxidase-like property of PANI-MnO<sub>2</sub> was photometrically studied by using TMB as substrate. Typically, PANI-MnO<sub>2</sub> (30 μL, 1 g L<sup>-1</sup>) was added into 2.94 mL of acetate buffer (0.1 M, pH 4.0), followed by adding TMB (30 μL, 10 mM) and incubating the mixture for 2 min. Then,

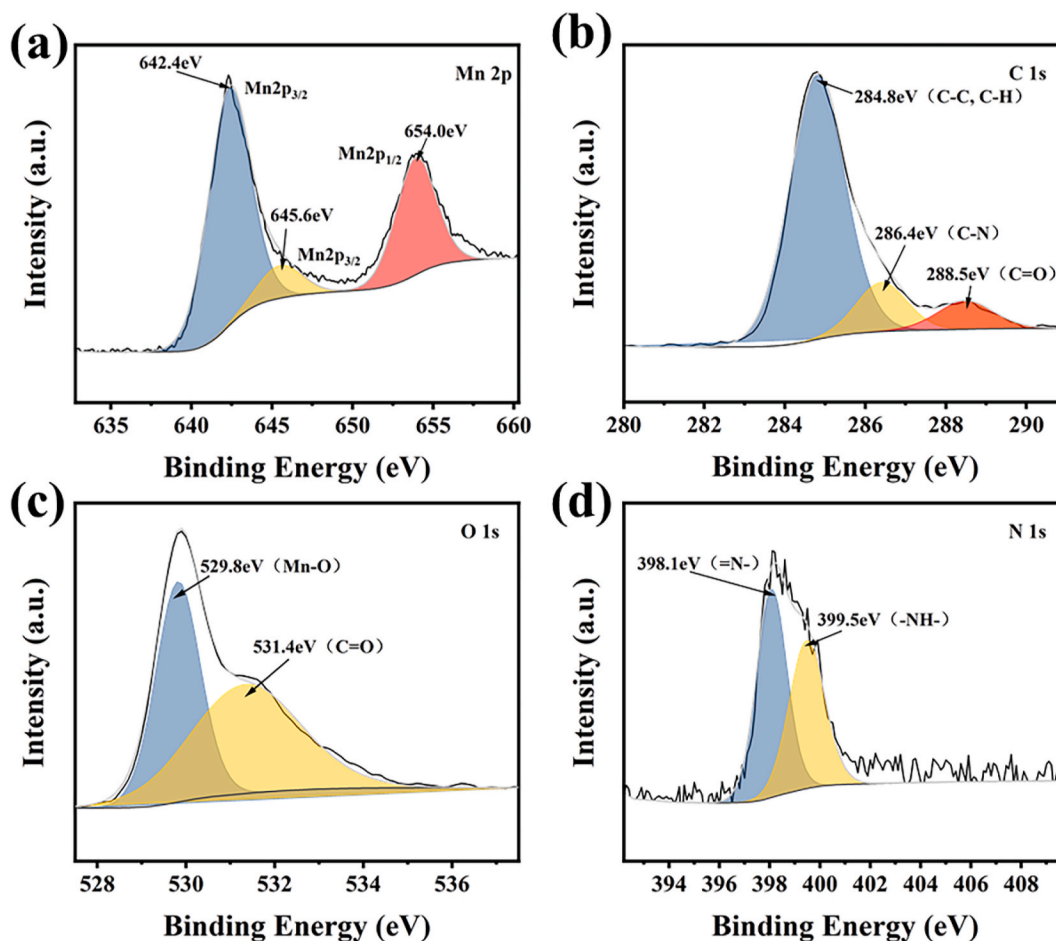


Fig. 2. The XPS spectrum of PANI-MnO<sub>2</sub>, (a) Mn 2p, (b) C 1s, (c) O 1s, and (d) N 1s.

the absorbance at 650 nm of the mixed solution was measured by UV-Vis immediately. The analysis process of MnO<sub>2</sub> and MnO<sub>2</sub> nano-sheets was performed similarly to that described above, but different for the addition amount was adjusted according to the test of manganese content by inductively coupled plasma mass spectrometry. Details can be seen in Table S1.

#### 2.4. Colorimetric detection of glyphosate

In order to detect glyphosate, different concentration of glyphosate reacted with ALP (100  $\mu$ L, 5.4 mg L<sup>-1</sup>), 100  $\mu$ L AAP (1.8 mM) and 100  $\mu$ L Tris-HCl (50 mM, pH 10.0) were added in 5 mL centrifuge tube and incubated at 37 °C for 60 min. After that, the product was supplemented with 2.54 mL of acetate buffer (0.1 M, pH 4.0) and PANI-MnO<sub>2</sub> (30  $\mu$ L, 1 g L<sup>-1</sup>). The centrifuge tube was shaken for 5 s to ensure adequate contact between the PANI-MnO<sub>2</sub> and AA, followed by adding TMB (30  $\mu$ L, 10 mM) to fulfill reaction in 2 min. Finally, recording the absorbance at 650 nm of the mixed solution.

To study the selectivity of colorimetric method for glyphosate, some possible interfering ions and pesticides were selected investigated in assay reaction. The subsequent treatment was similar to those of the detection of glyphosate.

#### 2.5. Analysis of real samples

The soil, tap water and lake water samples were obtained from near our lab and Lihu Lake. Agri-food products (pear, cucumber, soybean) were obtained from the local supermarket and stored at 4 °C before analysis. Each sample was spiked with 0  $\mu$ M, 5  $\mu$ M, 10  $\mu$ M glyphosate

and measured three times. The detailed sample pretreatment method was explained in the supplementary materials.

#### 2.6. Fabrication of colorimetric sensing platform

To achieve the on-site detection of OPS, the portable analytical platform was conducted on a 96-well plate to control natural light interference. This platform consisted of a LED lamp, a white paper partition, a mirror, an acrylic board and a smartphone holder. RGB values were extracted from the pictures taken by smartphone.

### 3. Results and discussion

#### 3.1. Characterizations of PANI-MnO<sub>2</sub>

The PANI were characterized with scanning electron microscope (SEM), PANI maintained uniform fibrous structure with a diameter of 30–50 nm and a length of several hundred of nanometers (Fig. S1). The TEM image in Fig. 1a showed that the PANI-MnO<sub>2</sub> was rod-shaped structure with a diameter between 70 and 80 nm. Compared with the PANI, the PANI-MnO<sub>2</sub> had a rougher surface, the PANI was wrapped by a thin layer of MnO<sub>2</sub> nanoparticles with a thickness of about 10–25 nm. The HR-TEM image (Fig. 1b) demonstrated uniform distribution of MnO<sub>2</sub> nanoparticles on PANI surface. They were potential active sites, which may play important roles in the catalytic reaction of PANI-MnO<sub>2</sub>. Fig. 1c showed lattice fringes of MnO<sub>2</sub> further confirm that the formation of MnO<sub>2</sub> nanoparticles. The elemental mapping (Fig. 1d–h) confirmed the homogeneous distribution of C, N, O and Mn in PANI-MnO<sub>2</sub>. Furthermore, the EDS results (Fig. S2a) were also indicated the

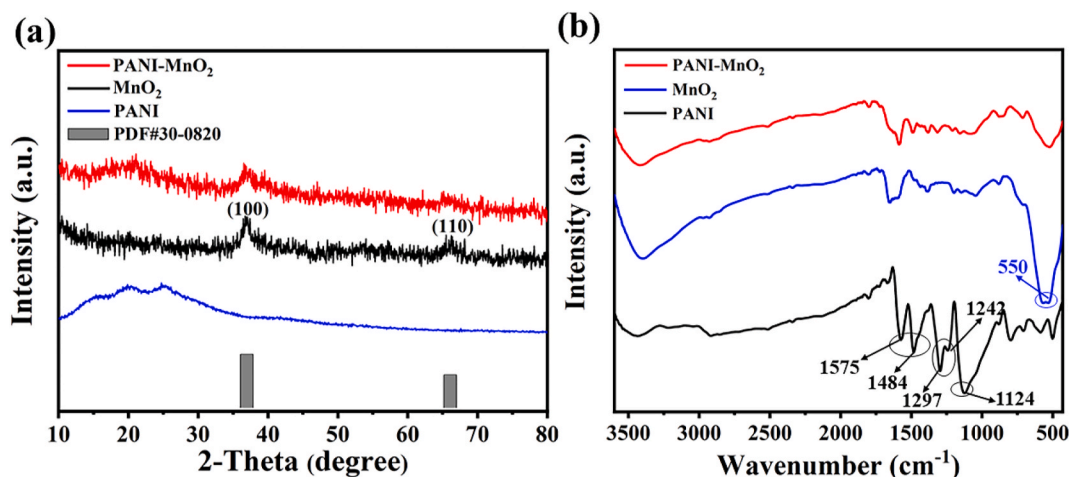


Fig. 3. (a) XRD patterns of PANI, MnO<sub>2</sub> and PANI-MnO<sub>2</sub>, respectively. (b) FTIR spectra of PANI, MnO<sub>2</sub> and PANI-MnO<sub>2</sub>, respectively.

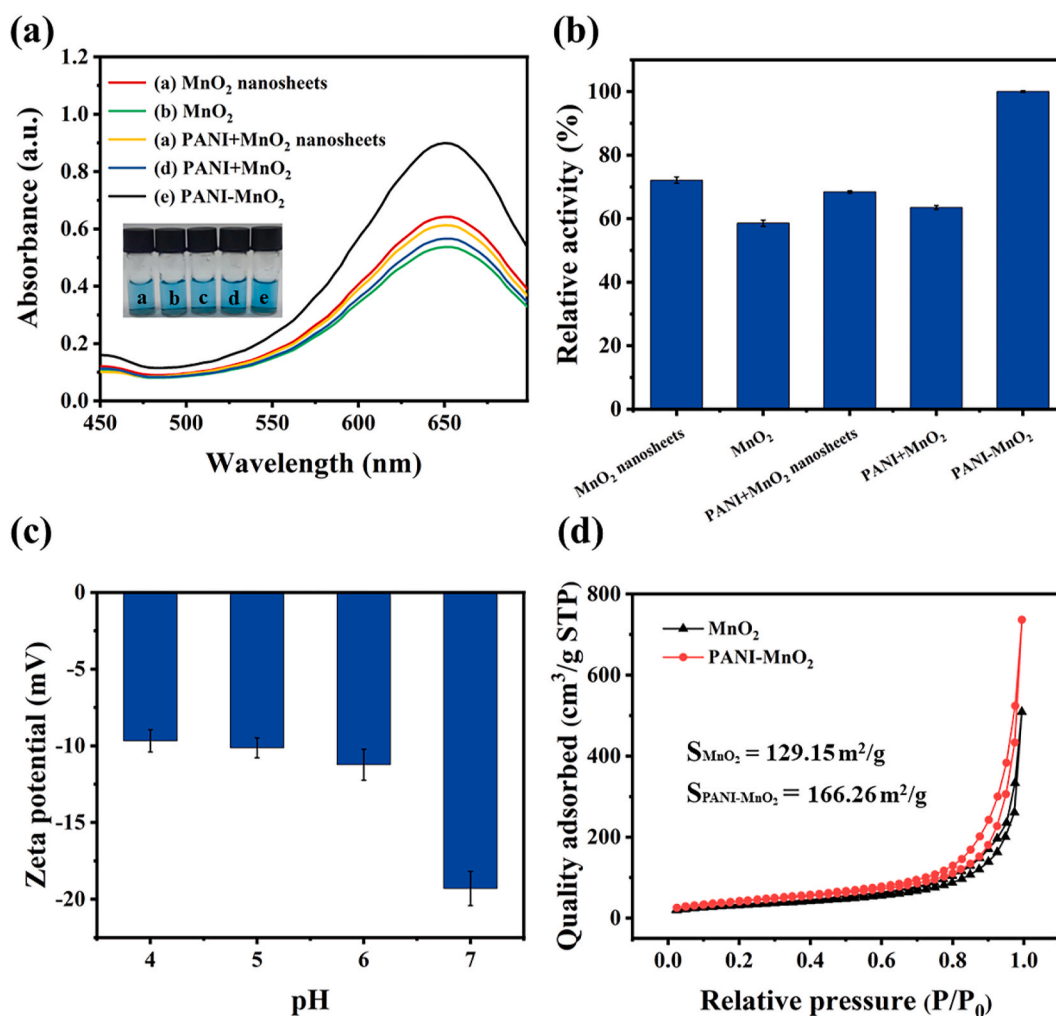


Fig. 4. (a) Comparison of absorption at 650 nm of nanozymes. (b) The relative activity was calculated by identifying the differential absorbance, activity of PANI-MnO<sub>2</sub> was set as 100 %. (c) The effect of pH on the zeta potential of PANI-MnO<sub>2</sub>. (d) N<sub>2</sub> adsorption-desorption isotherms of MnO<sub>2</sub> and PANI-MnO<sub>2</sub>.

presence of C, N, O and Mn elements.

X-ray photoelectron spectroscopy (XPS) was used to investigate the elemental and chemical composition of PANI-MnO<sub>2</sub>. The survey spectrum (Fig. S2b) again confirmed the co-existence of C, N, O and Mn elements in the PANI-MnO<sub>2</sub>. The Mn 2p peak (Fig. 2a) was composed of

two spin-orbit doublets, Mn 2p<sub>1/2</sub> with binding energy of 654.0 eV and Mn 2p<sub>3/2</sub> with binding energy of 642.4 and 645.6 eV. The typical characteristics of tetravalent Mn were in accordance with that previously reported [29]. The peak of C 1s can be deconvoluted into three peaks located at 284.8, 286.4 and 288.5 eV (Fig. 2b), which can be

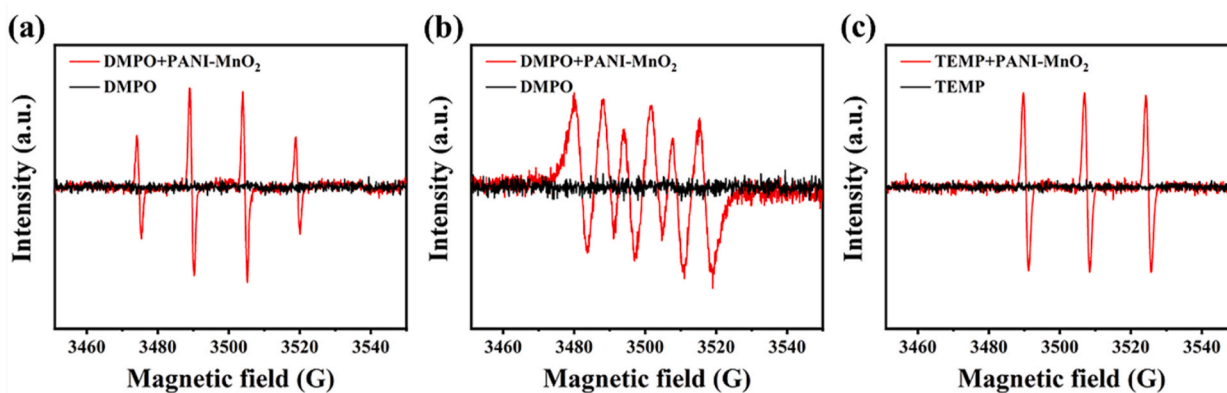


Fig. 5. The EPR spectra for (a)  $\bullet\text{OH}$ , (b)  $\text{O}_2^{\bullet-}$  and (c)  $^1\text{O}_2$  in the DMPO/TEMP + PANI-MnO<sub>2</sub> systems.

ascribed to C–C/C–H, C–N and C=O groups, respectively [30]. The O 1s spectrum (Fig. 2c) was attributed to two peaks of 529.8 eV (Mn–O) and 531.4 eV (C=O). Fig. 2d showed that the N 1s contribution at 398.1 and 399.5 eV, belonging to quinoid imine (=N–) and benzenoid amino group (–NH–), respectively [31].

The X-ray diffractometer patterns of PANI, MnO<sub>2</sub> and PANI-MnO<sub>2</sub> were displayed in Fig. 3a. The diffraction peaks at 20.4° and 25.0° in PANI were attributed to the periodicity of the polymer chain [32]. MnO<sub>2</sub> has two characteristic diffraction peaks located at 37.1° and 66.4°, corresponding to the (100) and (110) crystal planes of MnO<sub>2</sub>, respectively. They were identical to the hexagonal phase MnO<sub>2</sub> (PDF#30–0820). Similar peaks in PANI-MnO<sub>2</sub> were also observed clearly, but these diffraction peaks have decreased, indicating the presence of PANI and the formation MnO<sub>2</sub> nanoparticles shell [33].

Fourier transform infrared (FTIR) spectroscopy was used to examine the structures and composition of PANI, MnO<sub>2</sub> and PANI-MnO<sub>2</sub> (Fig. 3b). The prepared PANI presented the characteristic peaks at 1575, 1484, 1297, 1242, 1124 cm<sup>-1</sup>, which were corresponding to stretching of the benzenoid and quinonoid rings, C–N and C=N stretching vibrations and N = Q = N (where Q denoted the quinonoid ring) bending vibration, respectively [32]. The similar peaks at the analogous position were presented in PANI-MnO<sub>2</sub>, indicating the presence of PANI. Furthermore, the sharp peak at 550 cm<sup>-1</sup> should be caused by of the Mn–O vibrations, indicating the presence of MnO<sub>2</sub> [29].

### 3.2. Colorimetric response and possible catalytic mechanism of PANI-MnO<sub>2</sub>

Fig. 4a showed the absorbance of TMB in different catalytic systems (MnO<sub>2</sub> nanosheets, MnO<sub>2</sub>, PANI + MnO<sub>2</sub> nanosheets, PANI + MnO<sub>2</sub>, PANI-MnO<sub>2</sub>), the appearance of an absorbance signal at 650 nm and typical blue color indicated those nanozymes had intrinsic oxidase-like activities. From the relative activity of Fig. 4b, under the same conditions, the catalytic activity in the order PANI-MnO<sub>2</sub> > MnO<sub>2</sub> nanosheets > MnO<sub>2</sub>. In order to gain more insights into the oxidase-like activity of the PANI-MnO<sub>2</sub>, the steady-state kinetic experiment was carried out (Fig. S3). Using Lineweaver–Burk equation, Michaelis constant ( $K_m$ , 0.36 mM) and the maximum reaction velocity ( $V_{max}$ ,  $2.7 \times 10^{-7} \text{ M s}^{-1}$ ) were determined, indicating high binding affinity between TMB and PANI-MnO<sub>2</sub>. The differences of oxidase-like activity among these nanozymes were mainly caused by factors such as compositions, surface properties, morphologies, and electron transfer abilities [34].

In order to probe the catalytic mechanism of PANI-MnO<sub>2</sub>, the effects of surface and electrochemical properties on oxidase-like activity were studied. As depicted in Fig. 4c, the surface charge of PANI-MnO<sub>2</sub> was negative in acetate buffer. Under acidic conditions, TMB molecules ( $\text{p}K_a \approx 4.2$ ) became positively charged via protonation [34]. Therefore, PANI-MnO<sub>2</sub> might interact with TMB through electrostatic interactions, the TMB were more readily sorbed to PANI-MnO<sub>2</sub> surface, facilitating subsequent electron transfer. The N<sub>2</sub> adsorption/desorption isotherm curves of MnO<sub>2</sub> and PANI-MnO<sub>2</sub> (Fig. 4d) exhibited type V adsorption/desorption behavior, which was ascribed to the existence of the mesoporous structure. Compared with MnO<sub>2</sub>, due to PANI as carriers

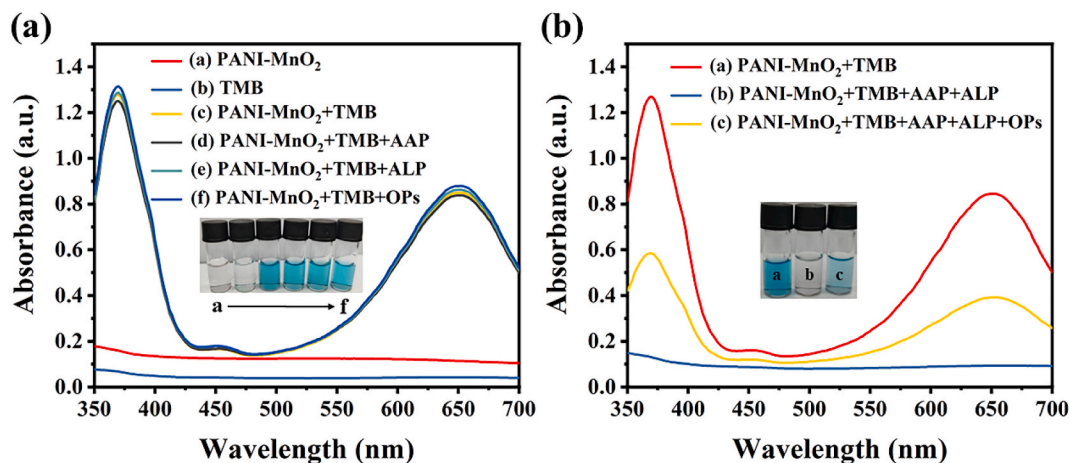


Fig. 6. (a) Absorption spectral observation of PANI-MnO<sub>2</sub> oxidase mimetics activity. Inset: Solutions of different components under white light. (b) Absorption spectra of the different solutions of PANI-MnO<sub>2</sub> with TMB. Inset: Corresponding photographs under white light.

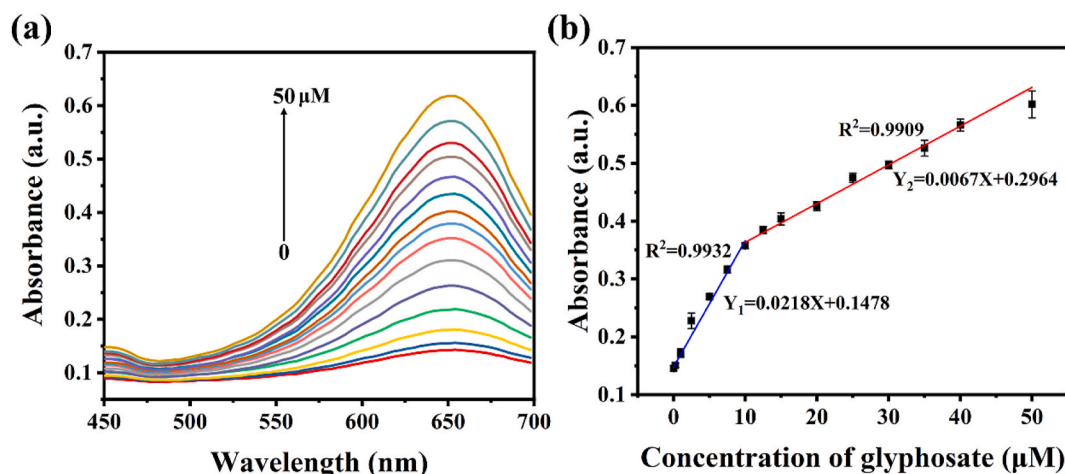


Fig. 7. (a) Difference of absorbance with different concentrations of glyphosate (0–50  $\mu\text{M}$ ). (b) The corresponding calibration graph for the detection of glyphosate.

prevented aggregation phenomenon of  $\text{MnO}_2$ , the specific surface area of PANI- $\text{MnO}_2$  was increased by 28.7 %. This implied that the PANI- $\text{MnO}_2$  possessed a higher catalytically active surface area and exposed more active sites.

The redox peak currents of the PANI- $\text{MnO}_2/\text{GCE}$  were higher than  $\text{MnO}_2$  nanosheets/ $\text{GCE}$  and  $\text{MnO}_2/\text{GCE}$  (Fig. S4a). In addition, the area of CV curves increased with the increase of scan rate while the shape of the CV curves kept almost unchanged (Fig. S4b). The results above illustrated that PANI- $\text{MnO}_2/\text{GCE}$  has better conductivity and cycling stability. It can be attributed to the extended conjugated  $\pi$  bonds of PANI, which improved the PANI- $\text{MnO}_2$  surface electrochemistry performance and accelerated the electron transfer rate [35]. Thus, the catalytic performance enhancement of PANI- $\text{MnO}_2$  can arise due to synergistic effects between PANI and  $\text{MnO}_2$ .

As shown in Fig. S5a, the absorbance of PANI- $\text{MnO}_2/\text{TMB}$  system increased by around 49 % in the  $\text{O}_2$ -saturated solution, and decreased by around 44 % in the  $\text{N}_2$ -saturated solution, indicating that dissolved  $\text{O}_2$  as substrate played an important role in PANI- $\text{MnO}_2$  catalysis process. Fig. S5b illustrated that the oxidase mimicking activity of PANI- $\text{MnO}_2$  was significantly suppressed by these quenchers (AA, TBA, FFA and PBQ). This demonstrated that PANI- $\text{MnO}_2$  could catalyze  $\text{O}_2$  to produce  $\bullet\text{OH}$ ,  $\text{O}_2^{\bullet-}$  and  $^1\text{O}_2$ . The EPR experiments further confirmed the generation of the  $\bullet\text{OH}$ ,  $\text{O}_2^{\bullet-}$  and  $^1\text{O}_2$ . Fig. 5a showed 1:2:2:1 quartet characteristic of DMPO- $\bullet\text{OH}$  in the presence, indicating that PANI- $\text{MnO}_2$  have an ability to generate hydroxyl radicals [36]. The typical EPR spectra confirmed the presence of the superoxide radicals (Fig. 5b). The EPR signal with an intensity ratio of 1:1:1 indicated the generation  $^1\text{O}_2$  (Fig. 5c).

### 3.3. Principle of colorimetric sensing strategy

To explore the colorimetric sensing mechanism, the UV-Vis spectrophotometer was used to monitor changes in absorbance during the reaction. From the absorption spectra and photographs of Fig. 6a, it can be seen that the solutions of PANI- $\text{MnO}_2$  and TMB were colorless and there was no absorbance generated near 650 nm, indicating that the TMB alone was not oxidized under natural light conditions. The mixture of PANI- $\text{MnO}_2$  and TMB turned blue, and the absorbance significantly increased. Meanwhile, the PANI- $\text{MnO}_2/\text{TMB}$  color reaction system has been found to be unaffected by the presences of OPs, AAP and ALP. However, when PANI- $\text{MnO}_2$  and TMB are incubated with ALP and AAP, a significant decrease of oxidase-like activity was observed accompanied by an attenuated catalytic efficiency of PANI- $\text{MnO}_2$  toward TMB (Fig. 6b). When glyphosate was incubated with ALP and AAP, and then added into the mixture of PANI- $\text{MnO}_2/\text{TMB}$ , the value of absorption increased and the blue color restored. We concluded that glyphosate

could irreversibly inhibit the activity of ALP and hinder subsequent reactions [37], loss of AA caused extra PANI- $\text{MnO}_2$  preservation and absorbance recovery [38]. Thus, the above results demonstrated that principle of detecting OPs was feasible.

### 3.4. Optimization of experimental conditions

To obtain higher sensitivity and wider linear range, detection conditions were investigated such as the pH of the buffer, enzyme reaction time and temperature, ALP concentration and AAP concentration. The reaction time was fixed at 60 min to optimize the pH of the buffer.  $A_0$ -A was used as a criterion to optimize the detection conditions.  $A_0$  and A represented the absorbance of PANI- $\text{MnO}_2/\text{TMB}$  color reaction system at 650 nm in the absence and presences of  $180 \mu\text{g L}^{-1}$  ALP and  $60 \mu\text{M}$  AAP, respectively. The values of  $A_0$ -A increased as the enzymatic reaction progressed and reached the stationary state at around 60 min (Fig. S6a). Hence, the optimal enzymatic reaction time was believed to be 60 min. The value of  $A_0$ -A was maximal at pH 10.0 (Fig. S6b). The ALP exhibited promising catalytic activity against AAP in alkaline environments. However, excessive pH values were also detrimental to the enzyme activity [39]. Similarly, the incubation temperature was  $37^\circ\text{C}$ , the value of  $A_0$ -A reached maximum value (Fig. S6c). Therefore, the optimum pH of enzymatic reaction was 10.0, and the optimum temperature was  $37^\circ\text{C}$ . In addition, the PANI- $\text{MnO}_2$  displayed the highest oxidase-like activity at pH 4.0 (Fig. S6d). Therefore, pH 4.0 was chosen as the optimal pH for subsequent colorimetric analysis.

The sensitivity of glyphosate detection was related to its relative inhibition rate. High or low concentrations of ALP and AAP were unfavorable to detection of glyphosate. If the enzyme reaction rate was too fast, the glyphosate was too late to inhibit the activity of ALP. In case the enzyme reaction rate was too low, resulting in higher value of absorbance, which affected the detection effect. As shown in Figs. S6e and S6f, when the concentration of AAP was changed from 0 to  $60 \mu\text{M}$  and the concentration of ALP was varied from 0 to  $180 \mu\text{g L}^{-1}$ , and the relative inhibition rate of glyphosate on activity of ALP increased with increasing concentrations of ALP and AAP. Subsequently, the relative inhibition rate decreased. Therefore, and  $60 \mu\text{M}$  of AAP and  $180 \mu\text{g L}^{-1}$  of ALP were chosen for the subsequent colorimetric detection.

The relative inhibition rate was calculated using the equation:  $(A_{\text{GLY}} - A) / A_{\text{GLY}} \times 100\%$ .  $A_{\text{GLY}}$  was value of absorbance in the presence of the  $10 \mu\text{M}$  glyphosate, and A was the value of absorbance at 650 nm without glyphosate.

### 3.5. Detection of glyphosate

The PANI- $\text{MnO}_2/\text{TMB}$  system was established to detect glyphosate

**Table 1**  
Comparison with earlier reported colorimetric glyphosate sensing methods.

Sensing materials	Linear range ( $\mu\text{M}$ )	LOD ( $\mu\text{M}$ )	Application	References
CS <sub>2</sub>	21.89–47.33	6.51	Soil, wheat	[40]
Cu(II)-PV	2.5–60	2.66	Tap water	[41]
Cu(II)	2.00–200	1.00	Soil, environmental water	[42]
MoS <sub>2</sub> nanoflake	2.37–11.8	0.51	Environmental water	[43]
PANI-MnO <sub>2</sub>	0.50–50	0.39	Soil, water samples, fruit	This paper

under optimal conditions. The absorption signal was recorded in Fig. 7a. As the glyphosate concentration increased, the absorbance decreased linearly. In the range of glyphosate concentration from 0.50 to 50  $\mu\text{M}$ , as the glyphosate concentration increased,  $A_{650}$  (the value of absorbance at 650 nm) increased gradually. Showing two-segment piecewise linear function (Fig. 7b).  $A_{650}$  values showed a linear relationship with glyphosate concentration from 0.25 to 10  $\mu\text{M}$ . The linear equation can be expressed as follows:  $Y_1 = 0.0218X + 0.1478$  ( $R^2 = 0.9932$ , X represented concentration of glyphosate). There was a linear relationship between  $A_{650}$  and glyphosate concentration in the range of 10–50  $\mu\text{M}$ . The equation can be expressed as follows:  $Y_2 = 0.0067X + 0.2964$  ( $R^2 = 0.9909$ ). The limit of detection (LOD) of the nanozyme colorimetric sensing method was 0.39  $\mu\text{M}$  ( $S/N = 3$ ). As shown in Table 1, compared with previous work, the proposed colorimetric method has a better linear response range and lower detection limit.

Furthermore, the effects of potential interferences were performed to examine the selectivity of sensing method. Specifically, the influence of some common substances including metal ions ( $\text{Na}^+$ ,  $\text{K}^+$ ,  $\text{Mg}^{2+}$ ,  $\text{Cu}^{2+}$ ,  $\text{Ca}^{2+}$ ,  $\text{Al}^{3+}$ ) and anions ( $\text{Cl}^-$ ,  $\text{SO}_4^{2-}$ ,  $\text{NO}_3^-$ ,  $\text{NO}_2^-$ ,  $\text{CO}_3^{2-}$ ,  $\text{HCO}_3^-$ ) were investigated. As shown in Fig. 8a, either metal ions or anions have little or no effects on the absorption signal.

The selectivity of proposed method toward glyphosate has been further examined by monitoring eight common pesticides (dipterex, rogor, chlorpyrifos, carbendazim, thiabendazole, dinotefuran, imidacloprid and thiamethoxam). OPs (dipterex, rogor, chlorpyrifos) can generate absorbance signals due to their own phosphate ester structure, other pesticides did not have the such characteristics and could not cause any disturbance in detection (Fig. 8b), indicating that the proposed method showed good selectivity toward OPs.

### 3.6. Determination of glyphosate in real samples

To explore the practical usability of the proposed colorimetric method, we determined the glyphosate concentration in tap water, lake water, soil, pear, soybean and cucumber. Among them, OPs were detected in the soybean sample, but was not detected in the other samples. As displayed in Table 2, the results obtained from our experiments agreed well with the specifications. Furthermore, the recovery was in the range of 98.4–108.6 %, and the relative standard deviation (RSD) was within the range of 0.6–3.7 %. All the results indicated the feasibility of the proposed for detecting glyphosate in practical samples.

### 3.7. Building a colorimetric smartphone-based platform for detection of glyphosate

Our proposed colorimetric method by using PANI-MnO<sub>2</sub> can well detect glyphosate, but still required analytical instruments. To further improve the utility of this method, the colorimetric platform was established. The 3D design of the colorimetric platform was shown in Scheme 2A. The LED light with a white paper partition provided appropriate light intensity to illuminate the 96-well plate, while the transparent acrylic plate was used to support the 96-well plate. A mirror

**Table 2**  
Determination of glyphosate in real samples (n = 3).

Samples	Added( $\mu\text{M}$ )	Found( $\mu\text{M}$ )	Recovery(%)	RSD(%)
Tap water	0	ND <sup>1</sup>	–	–
	5	5.18	103.6	1.5
	10	9.86	98.6	2.3
Lake water	0	ND	–	–
	5	5.12	102.3	2.4
	10	9.95	99.5	2.0
Soil	0	ND	–	–
	5	4.98	99.6	2.1
	10	10.25	102.5	3.7
Pear	0	ND	–	–
	5	4.92	98.4	2.2
	10	9.92	99.2	0.7
Cucumber	0	ND	–	–
	5	5.22	104.5	2.1
	10	9.87	98.7	0.6
Soybean	0	3.37	–	1.7
	5	8.8	108.6	1.5
	10	13.87	105.0	2.6

ND<sup>1</sup>: Not detected.

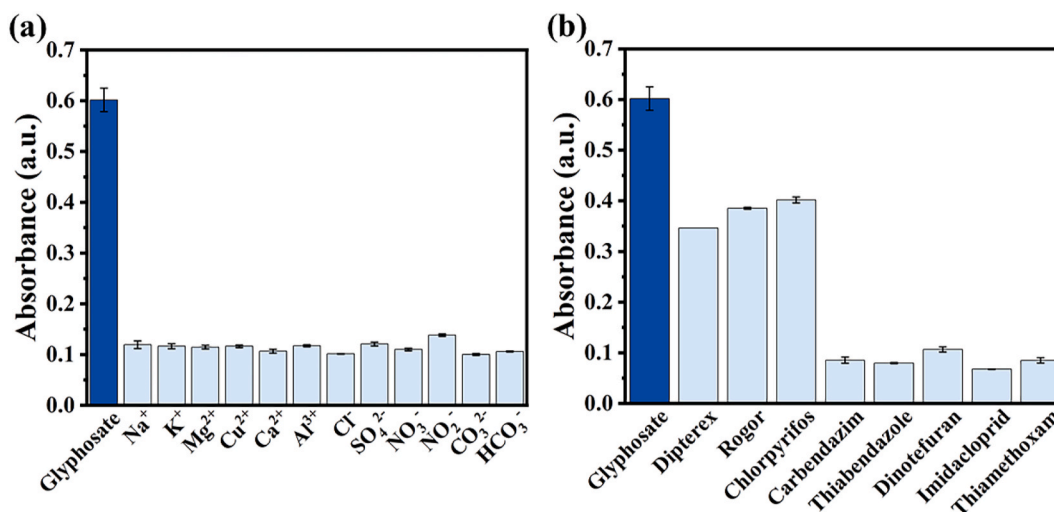
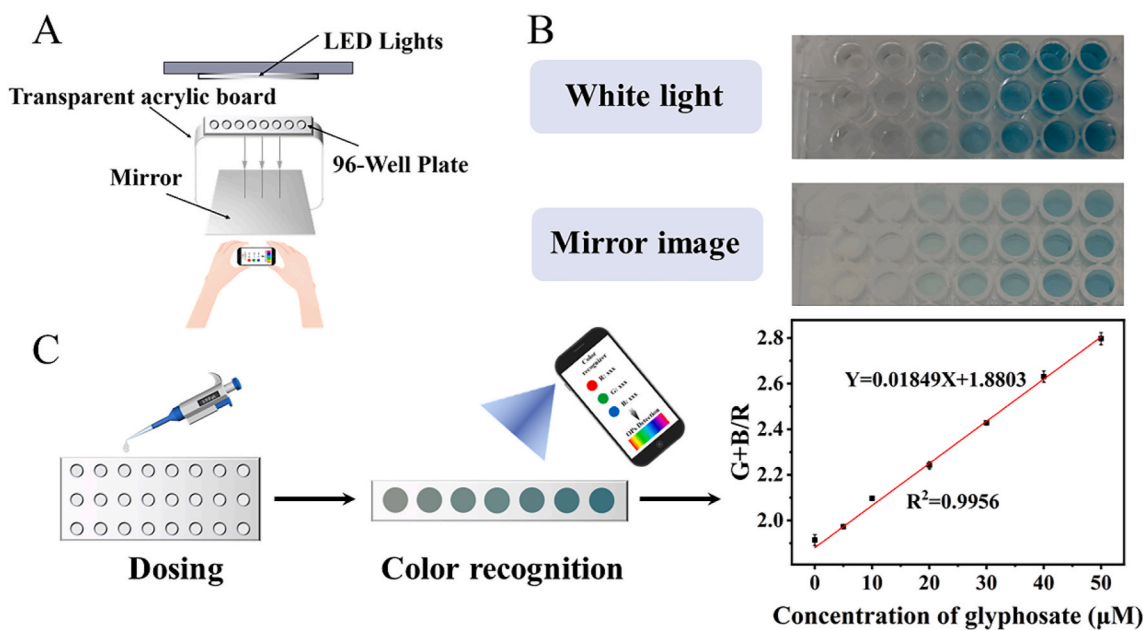


**Fig. 8.** (a) Absorbance response of assay system solutions in the presence of common coexistence ions (100  $\mu\text{M}$  each). (b) Absorbance response of assay system solutions in the presence of different pesticides (100  $\mu\text{M}$  each).



**Scheme 2.** The mechanism and 3D design of the colorimetric platform based on a smartphone for the detection of glyphosate.

was arranged at the bottom of the acrylic board, and the color of the solution in the 96-well plate was reflected on the smartphone camera by the mirror. Compared to photos taken under white light conditions with nonuniform colors, this simple arrangement of the device allowed us to obtain clearer images (Scheme 2B).

The specific on-site detection process was shown in Scheme 2C. With the addition of glyphosate, the colorimetric sensing platform would display a color change from light blue to deep blue. After taking photos with a smartphone, the smartphone APP (color recognizer) can monitor the absorbance change of the colorimetric reaction after processing in RGB value mode. The inset was the linear plot of the RGB values to the glyphosate concentration in the range of 5–50  $\mu\text{M}$  ( $(G + B)/R = 0.01849X + 1.8803$ ,  $R^2 = 0.9956$ ), the LOD was approximately at 1.2  $\mu\text{M}$  ( $S/N = 3$ ). The concentration of glyphosate in real samples (tap water, lake water, soil, pear, soybean and cucumber) was tested using the colorimetric sensing platform (Fig. S7 and Table S2), the recovery was in the range of 86.4–116.8 %, and the RSD was within the range of 0.3–3.5 %. These results showed the great potential of colorimetric platform in on-site detection of glyphosate.

#### 4. Conclusion

In summary, the PANI-MnO<sub>2</sub> nanozymes were successfully synthesized by one-step self-assembly redox method at room temperature. Meanwhile, a sensitive, rapid, and reliable colorimetric method for detecting OPs was established by combining the excellent oxidase-like activity of PANI-MnO<sub>2</sub> and the redox reaction between its and natural enzyme products. The method has been successfully applied to the detection of OPs in soil, water samples and agricultural products. In addition, a portable colorimetric sensing platform based on smartphone has been developed, which can realize the detection of OPs without the requirement of any sophisticated instrumental and overcome the uneven color distribution problem in traditional paper-based devices.

#### CRedit authorship contribution statement

**Cheng-Lin Yang:** Conceptualization, Validation, Methodology, Investigation, Writing – original draft. **Li-Hong Yu:** Conceptualization, Methodology, Data curation. **Yue-Hong Pang:** Conceptualization, Methodology, Formal analysis, Writing – review & editing, Funding

acquisition. **Xiao-Fang Shen:** Conceptualization, Resources, Project design, Funding acquisition, Supervision.

#### Declaration of competing interest

The authors declare no potential competing interests in this paper.

#### Data availability

Data will be made available on request.

#### Acknowledgments

This work was supported by the National Natural Science Foundation of China (22076067, 22276077).

#### Appendix A. Supplementary data

Supplementary data to this article can be found online at <https://doi.org/10.1016/j.aca.2023.342045>.

#### References

- [1] X. Wu, P. Wang, S. Hou, P. Wu, J. Xue, Fluorescence sensor for facile and visual detection of organophosphorus pesticides using AIE fluorogens-SiO<sub>2</sub>-MnO<sub>2</sub> sandwich nanocomposites, *Talanta* 198 (2019) 8–14.
- [2] R. Bala, M. Kumar, K. Bansal, R.K. Sharma, N. Wangoo, Ultrasensitive aptamer biosensor for malathion detection based on cationic polymer and gold nanoparticles, *Biosens. Bioelectron.* 85 (2016) 445–449.
- [3] J. Wang, J. Zhang, J. Wang, G. Fang, J. Liu, S. Wang, Fluorescent peptide probes for organophosphorus pesticides detection, *J. Hazard Mater.* 389 (2020), 122074.
- [4] B. Liu, Y. Ge, Y. Zhang, Y. Song, Y. Lv, X. Wang, S. Wang, Production of the class-specific antibody and development of direct competitive ELISA for multi-residue detection of organophosphorus pesticides, *Food Agr. Immunol.* 23 (2012) 157–168.
- [5] A. Juan-García, G. Font, C. Juan, Y. Picó, Pressurised liquid extraction and capillary electrophoresis–mass spectrometry for the analysis of pesticide residues in fruits from Valencian markets, Spain, *Food Chem.* 120 (2010) 1242–1249.
- [6] J.J. Grandy, E. Boyaci, J. Pawliszyn, Development of a carbon mesh supported thin film microextraction membrane as a means to lower the detection limits of benchtop and portable GC/MS instrumentation, *Anal. Chem.* 88 (2016) 1760–1767.
- [7] M.M. Gomez-Ramos, C. Ferrer, O. Malato, A. Aguera, A.R. Fernandez-Alba, Liquid chromatography-high-resolution mass spectrometry for pesticide residue analysis in fruit and vegetables: screening and quantitative studies, *J. Chromatogr. A* 1287 (2013) 24–37.

- [8] F. Liu, T. Lei, Y. Zhang, Y. Wang, Y. He, A BCNO QDs-MnO<sub>2</sub> nanosheets based fluorescence "off-on-off" and colorimetric sensor with smartphone detector for the detection of organophosphorus pesticides, *Anal. Chim. Acta* 1184 (2021), 339026.
- [9] J. Ge, L. Yang, Z. Li, Y. Wan, D. Mao, R. Deng, Q. Zhou, Y. Yang, W. Tan, A colorimetric smartphone-based platform for pesticides detection using Fe-N/C single-atom nanozyme as oxidase mimetics, *J. Hazard Mater.* 436 (2022), 129199.
- [10] P. Sawetwong, S. Chairam, P. Jarujamrus, M. Amatatongchai, Enhanced selectivity and sensitivity for colorimetric determination of glyphosate using Mn-ZnS quantum dot embedded molecularly imprinted polymers combined with a 3D-microfluidic paper-based analytical device, *Talanta* 225 (2021), 122077.
- [11] Z. Shen, D. Xu, G. Wang, L. Geng, R. Xu, G. Wang, Y. Guo, X. Sun, Novel colorimetric aptasensor based on MOF-derived materials and its applications for organophosphorus pesticides determination, *J. Hazard Mater.* 440 (2022), 129707.
- [12] M. Fu, F. Xu, J. Yan, C. Wang, G. Fan, G. Song, B. Chai, Mixed valence state cerium metal organic framework with prominent oxidase mimicking activity for ascorbic acid detection: mechanism and performance, *Colloid. Surface.* 641 (2022), 128610.
- [13] Z. Lin, X. Zhang, S. Liu, L. Zheng, Y. Bu, H. Deng, R. Chen, H. Peng, X. Lin, W. Chen, Colorimetric acid phosphatase sensor based on MoO<sub>3</sub> nanozyme, *Anal. Chim. Acta* 1105 (2020) 162–168.
- [14] P. Ni, S. Liu, B. Wang, C. Chen, Y. Jiang, C. Zhang, J. Chen, Y. Lu, Light-responsive Au nanoclusters with oxidase-like activity for fluorescent detection of total antioxidant capacity, *J. Hazard Mater.* 411 (2021), 125106.
- [15] X. Zhang, X. Mao, S. Li, W. Dong, Y. Huang, Tuning the oxidase mimics activity of manganese oxides via control of their growth conditions for highly sensitive detection of glutathione, *Sensor. Actuator. B Chem.* 258 (2018) 80–87.
- [16] Y. Wan, P. Qi, D. Zhang, J. Wu, Y. Wang, Manganese oxide nanowire-mediated enzyme-linked immunosorbent assay, *Biosens. Bioelectron.* 33 (2012) 69–74.
- [17] Z. Ma, Y. Xu, P. Li, D. Cheng, X. Zhu, M. Liu, Y. Zhang, Y. Liu, S. Yao, Self-catalyzed surface reaction-induced fluorescence resonance energy transfer on cysteine-Stabilized MnO<sub>2</sub> quantum dots for selective detection of dopamine, *Anal. Chem.* 93 (2021) 3586–3593.
- [18] X. Xu, R. Liu, Y. Cui, X. Liang, C. Lei, S. Meng, Y. Ma, Z. Lei, Z. Yang, PANI/FeUiO-66 nanohybrids with enhanced visible-light promoted photocatalytic activity for the selectively aerobic oxidation of aromatic alcohols, *Appl. Catal. B Environ.* 210 (2017) 484–494.
- [19] X.F. Lu, X.Y. Chen, W. Zhou, Y.X. Tong, G.R. Li,  $\alpha$ -Fe<sub>2</sub>O<sub>3</sub>@PANI core-shell nanowire arrays as negative electrodes for asymmetric supercapacitors, *ACS Appl. Mater. Inter.* 7 (2015) 14843–14850.
- [20] L. Ren, G. Zhang, Z. Yan, L. Kang, H. Xu, F. Shi, Z. Lei, Z.H. Liu, Three-Dimensional tubular MoS<sub>2</sub>/PANI hybrid electrode for high rate performance supercapacitor, *ACS Appl. Mater. Inter.* 7 (2015) 28294–28302.
- [21] J.X. Feng, L.X. Ding, S.H. Ye, X.J. He, H. Xu, Y.X. Tong, G.R. Li, Co(OH)<sub>2</sub> @PANI hybrid nanosheets with 3D networks as high-performance electrocatalysts for hydrogen evolution reaction, *Adv. Mater.* 27 (2015) 7051–7057.
- [22] X. Lu, W. Zhang, C. Wang, T.-C. Wen, Y. Wei, One-dimensional conducting polymer nanocomposites: synthesis, properties and applications, *Prog. Polym. Sci.* 36 (2011) 671–712.
- [23] X.F. Lu, X.J. Bian, Z.C. Li, D.M. Chao, C. Wang, A facile strategy to decorate Cu<sub>9</sub>S<sub>8</sub> nanocrystals on polyaniline nanowires and their synergetic catalytic properties, *Sci. Rep.* 3 (2013) 2955.
- [24] W. Song, M. Chi, M. Gao, B. Zhao, C. Wang, X. Lu, Self-assembly directed synthesis of Au nanorices induced by polyaniline and their enhanced peroxidase-like catalytic properties, *J. Mater. Chem. C* 5 (2017) 7465–7471.
- [25] D. Navadeepthy, M. Thangapandian, C. Viswanathan, N. Ponpandian, A nanocomposite of NiFe<sub>2</sub>O<sub>4</sub>-PANI as a duo active electrocatalyst toward the sensitive colorimetric and electrochemical sensing of ascorbic acid, *Nanoscale Adv.* 2 (2020) 3481–3493.
- [26] J. Huang, R.B. Kaner, Nanofiber formation in the chemical polymerization of aniline: a mechanistic study, *Angew. Chem. Int. Ed.* 43 (2004) 5817–5821.
- [27] L. Yuan, Z. Gan, Y. Fan, F. Ding, X. Xu, X. Chen, X. Zou, W. Zhang, Thermal-controlled active sensor module using enzyme-regulated UiO-66-NH<sub>2</sub>/MnO<sub>2</sub> fluorescence probe for total organophosphorus pesticide determination, *J. Hazard Mater.* 436 (2022), 129111.
- [28] T. Yao, A. Liu, Y. Liu, M. Wei, W. Wei, S. Liu, Ratiometric fluorescence sensor for organophosphorus pesticide detection based on opposite responses of two fluorescence reagents to MnO<sub>2</sub> nanosheets, *Biosens. Bioelectron.* 145 (2019), 111705.
- [29] J. Zhang, D. Shu, T. Zhang, H. Chen, H. Zhao, Y. Wang, Z. Sun, S. Tang, X. Fang, X. Cao, Capacitive properties of PANI/MnO<sub>2</sub> synthesized via simultaneous-oxidation route, *J. Alloy. Compd.* 532 (2012) 1–9.
- [30] K. Ghosh, C.Y. Yue, M.M. Sk, R.K. Jena, Development of 3-D Urchin-shaped coaxial MnO<sub>2</sub>@PANI composite and self-assembled 3-D Pillared Graphene foam for asymmetric all-Solid-state flexible supercapacitor application, *ACS Appl. Mater. Inter.* 9 (2017) 15350–15363.
- [31] Y. Zhang, X. Liu, L. Wu, W. Dong, F. Xia, L. Chen, N. Zhou, L. Xia, Z.-Y. Hu, J. Liu, H.S.H. Mohamed, Y. Li, Y. Zhao, L. Chen, B.-L. Su, A flexible, hierarchically porous PANI/MnO<sub>2</sub> network with fast channels and an extraordinary chemical process for stable fast-charging lithium-sulfur batteries, *J. Mater. Chem. A* 8 (2020) 2741–2751.
- [32] X. Lu, H. Mao, D. Chao, W. Zhang, Y. Wei, Fabrication of polyaniline nanostructures under Ultrasonic irradiation: from nanotubes to nanofibers, *Macromol. Chem. Phys.* 207 (2006) 2142–2152.
- [33] M. Chi, Y. Zhu, L. Jing, C. Wang, X. Lu, Fabrication of oxidase-like polyaniline-MnO<sub>2</sub> hybrid nanowires and their sensitive colorimetric detection of sulfite and ascorbic acid, *Talanta* 191 (2019) 171–179.
- [34] Q. Chen, S. Li, Y. Liu, X. Zhang, Y. Tang, H. Chai, Y. Huang, Size-controllable Fe-N/C single-atom nanozyme with exceptional oxidase-like activity for sensitive detection of alkaline phosphatase, *Sensor. Actuator. B Chem.* 305 (2020), 127511.
- [35] R. Saravanan, E. Sacari, F. Gracia, M.M. Khan, E. Mosquera, V.K. Gupta, Conducting PANI stimulated ZnO system for visible light photocatalytic degradation of coloured dyes, *J. Mol. Liq.* 221 (2016) 1029–1033.
- [36] Y. Chen, X. Long, R. Huang, I.Y. Zhang, G. Yao, B. Lai, Z. Xiong, Highly efficient electro-cocatalytic Fenton-like reactions for the degradation of recalcitrant naphthenic acids: exploring reaction mechanisms and environmental implications, *Chem. Eng. J.* 450 (2022), 138331.
- [37] F. Qu, H. Wang, J. You, Dual lanthanide-probe based on coordination polymer networks for ratiometric detection of glyphosate in food samples, *Food Chem.* 323 (2020), 126815.
- [38] Q. Zhao, T. Shen, Y. Liu, X. Hu, W. Zhao, Z. Ma, P. Li, X. Zhu, Y. Zhang, M. Liu, S. Yao, Universal nanoplatform for formaldehyde detection based on the oxidase-mimicking activity of MnO<sub>2</sub> nanosheets and the in Situ catalysis-Produced fluorescence Species, *J. Agr. Food Chem.* 69 (2021) 7303–7312.
- [39] J. Dong, H. Yang, Y. Li, A. Liu, W. Wei, S. Liu, Fluorescence sensor for organophosphorus pesticide detection based on the alkaline phosphatase-triggered reaction, *Anal. Chim. Acta* 1131 (2020) 102–108.
- [40] M.R. Jan, J. Shah, M. Muhammad, B. Ara, Glyphosate herbicide residue determination in samples of environmental importance using spectrophotometric method, *J. Hazard Mater.* 169 (2009) 742–745.
- [41] P. Yadav, F. Zelder, Detection of glyphosate with a copper(II)-pyrocatechol violet based GlyPKit, *Anal. Methods* 13 (2021) 4354–4360.
- [42] Y. Chang, Z. Zhang, J. Hao, W. Yang, J. Tang, A simple label free colorimetric method for glyphosate detection based on the inhibition of peroxidase-like activity of Cu(II), *Sensor. Actuator. B Chem.* 228 (2016) 410–415.
- [43] Q. Chen, H. Chen, Z. Li, J. Pang, T. Lin, L. Guo, F. Fu, Colorimetric sensing of glyphosate in environmental water based on peroxidase mimetic activity of MoS<sub>2</sub> nanosheets, *J. Nanosci. and Nanotechnol.* 17 (2017) 5730–5734.